Supplementary Materials:

- Supplementary Figures 1-6
- Supplementary Videos 1-2
- Supplementary Table 1

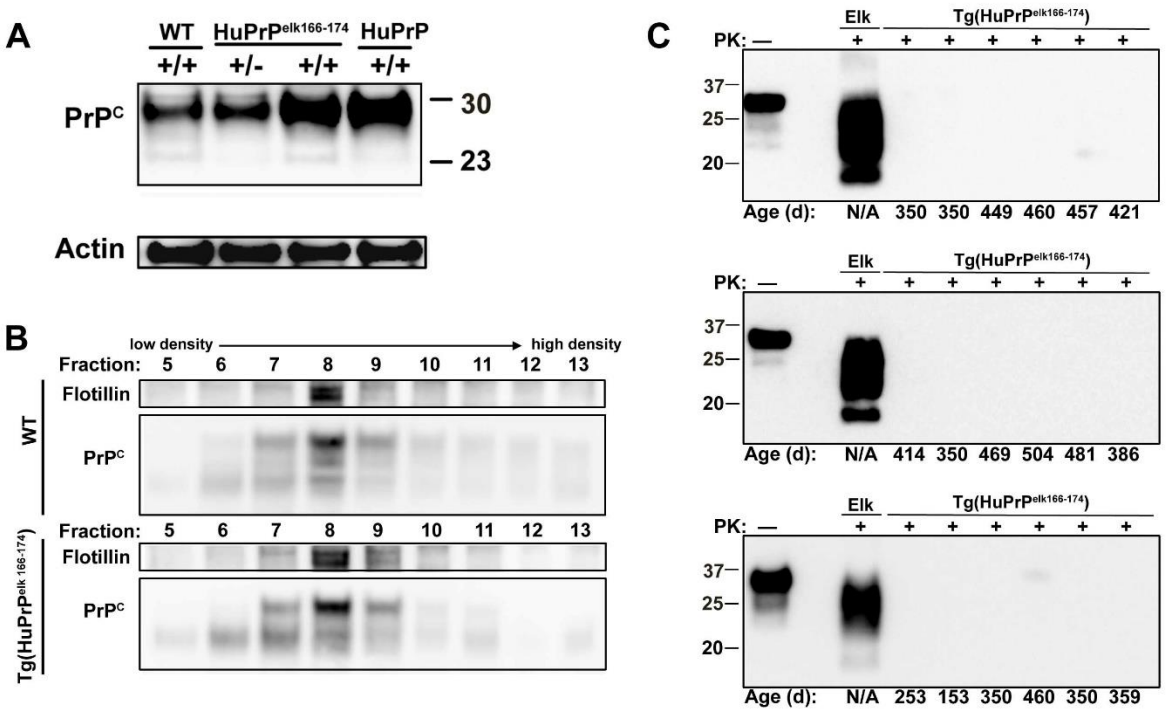

Supplemental Figure 1. Characterization of Tg(HuPrP$^{elk166-174}$) mouse brain. (**A**) Relative PrP^{C} expression levels in brains of wild type, Tg(HuPrP$^{elk166-174}$) [homozygous (+/+) or hemizygous (+/-)], and Tg(HuPrP) mice. Western blots of brain homogenates (80 µg protein) show equivalent PrP levels in homozygous Tg(HuPrP$^{elk166-174}$) and Tg(HuPrP) mice. The actin loading control is shown below. (**B**) Flotation assay. Density gradient sedimentation of brain homogenate from a WT or Tg(HuPrP$^{elk166-174}$) mouse reveals co-segregation of PrP^{C} with the raft marker, flotillin. (**C**) Brain homogenates from aged transgenic HuPrP$^{elk166-174}$ mice (12 homozygous and 6 hemizygous shown) were PK-digested and show no detectable PrP^{Sc}. A CWD-infected elk sample serves as a positive control.

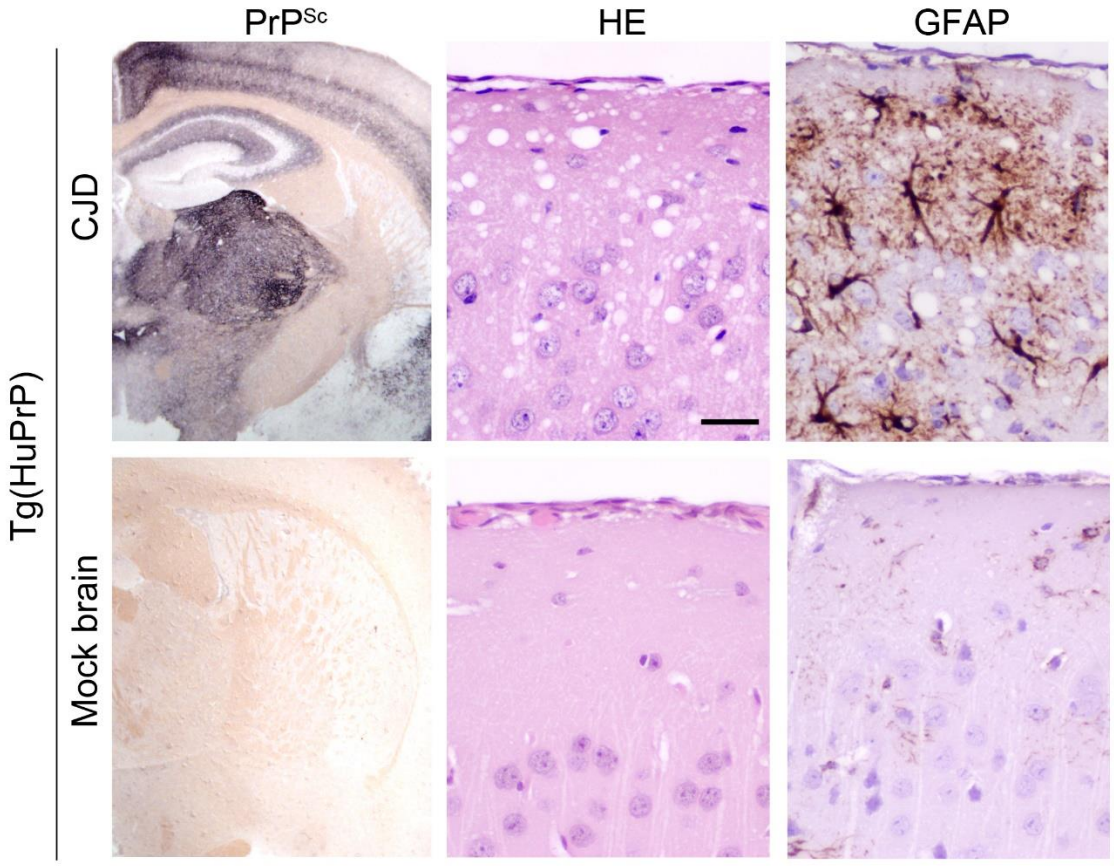

Supplemental Figure 2. Human CJD-infected transgenic mice. Brain sections from CJD-infected and mock-inoculated Tg(HuPrP) mice show the PrP^{Sc} distribution pattern in a paraffin-embedded tissue (PET) blot. The HE stained and GFAP-labelled sections show spongiosis and astrogliosis, respectively. Scale bar = 50 µm.

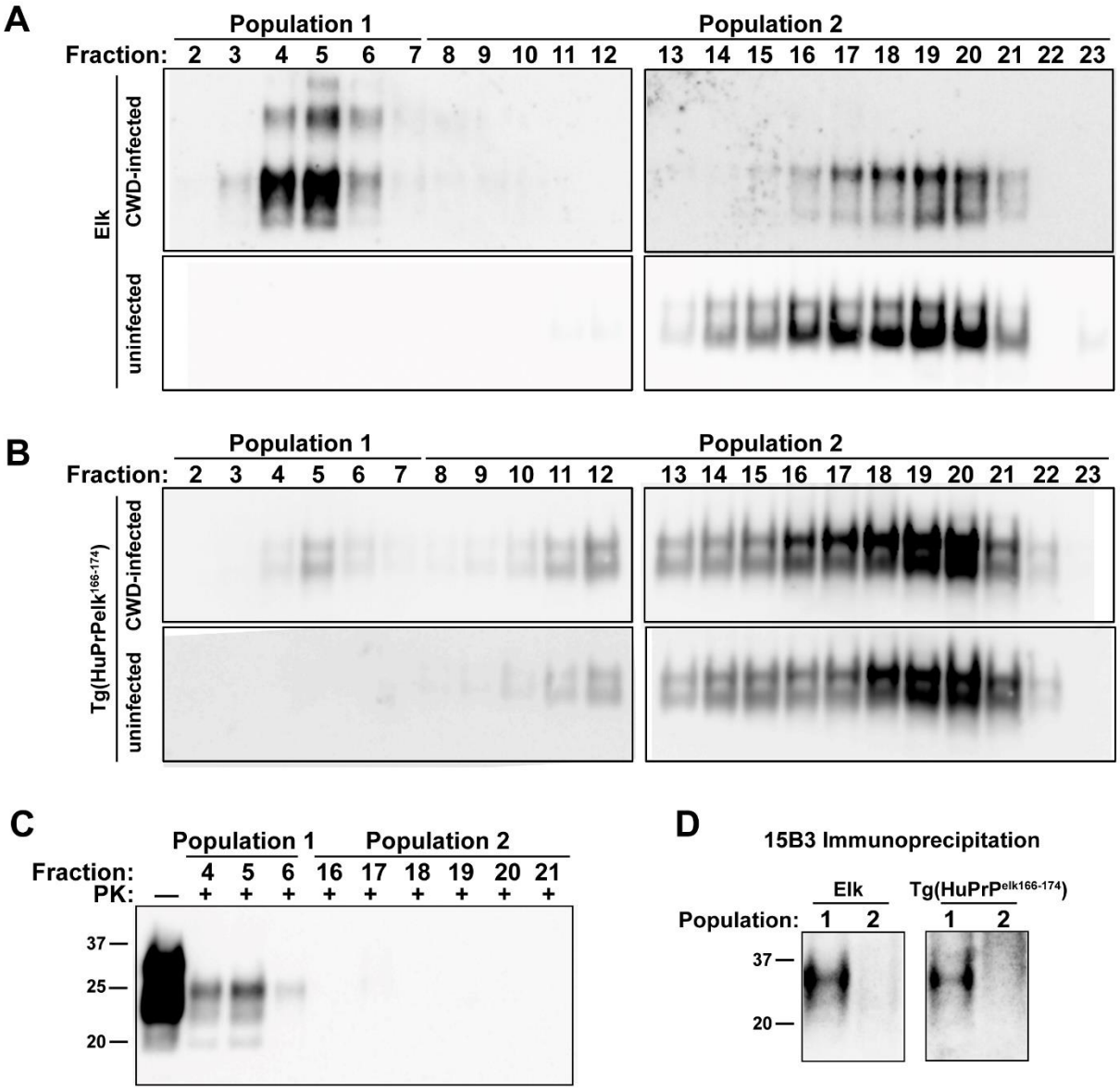

Supplemental Figure 3. PrP^{Sc} purification by centrifugation and size exclusion chromatography. FPLC fractions 2-23 from (**A**) CWD-infected or uninfected elk and (**B**) CWD-infected or uninfected Tg(HuPrP$^{elk166-174}$) mice revealed two distinct PrP populations in infected animals. (**C**) A Western blot of populations 1 and 2 from the CWD-infected elk revealed PK-resistant PrP^{Sc} in fractions 4-6, but not fractions 16-21. (**D**) Immunoprecipitation of pooled fractions comprising population 1 or population 2 using the PrP^{Sc}–specific antibody 15B3 shows PrP^{Sc} only in population 1.

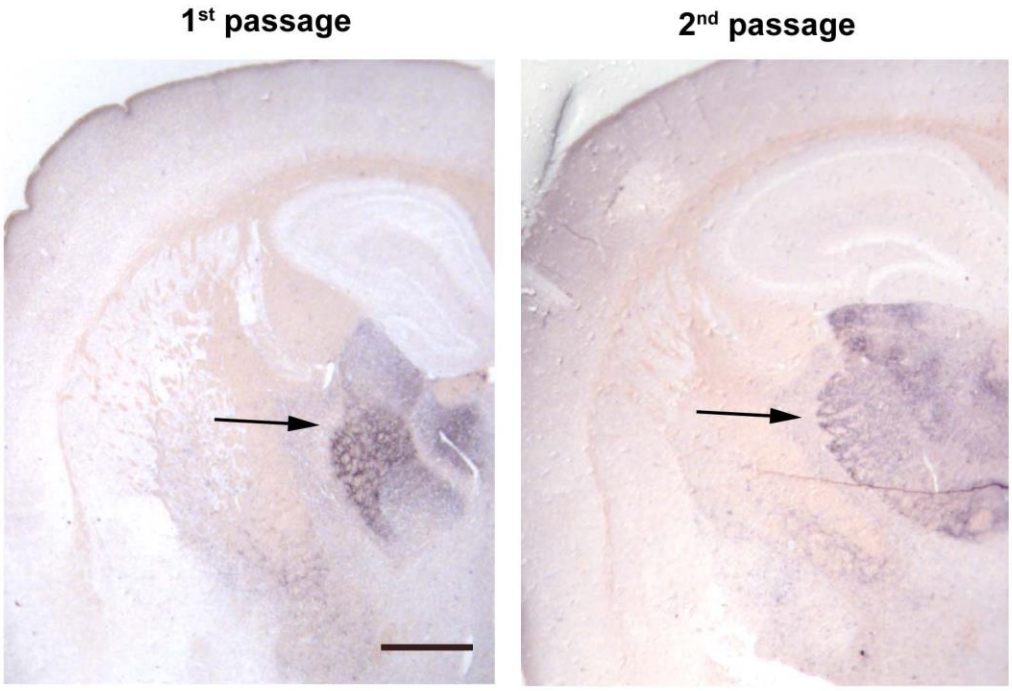

Supplemental Figure 4. No change in PrP^{Sc} deposition pattern upon sub-passage of CWD prions in Tg($HuPrP^{elk166-174}$) mice. PET blots from Tg($HuPrP^{elk166-174}$) mice infected with CWD reveal diffuse PrP^{Sc} deposition (arrows) in the thalamus of Tg($HuPrP^{elk166-174}$) mice during both the first and second passage of elk CWD in Tg($HuPrP^{elk166-174}$) mice. Scale bar = 1 mm.

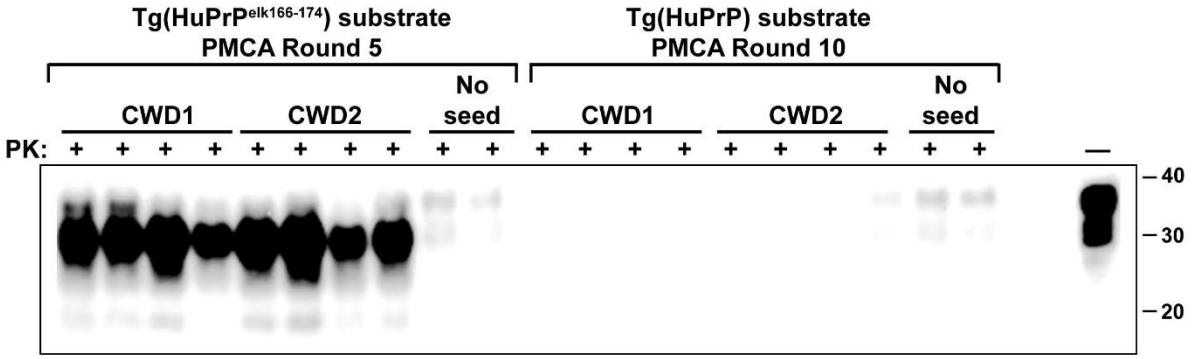

Supplemental Figure 5. CWD conversion of HuPrP$^{elk166-174}$ by protein misfolding cyclic amplification (PMCA). PMCA was used to test whether brain homogenate from Tg(HuPrP$^{elk166-174}$) or Tg(HuPrP) mice supports CWD prion conversion. Immunoblot shows conversion of HuPrP$^{elk166-174}$ by CWD after five rounds of PMCA. In contrast, no HuPrP was converted by CWD prions, even after 10 rounds of PMCA. Seed (CWD1 or CWD2) is indicated above replicate samples.

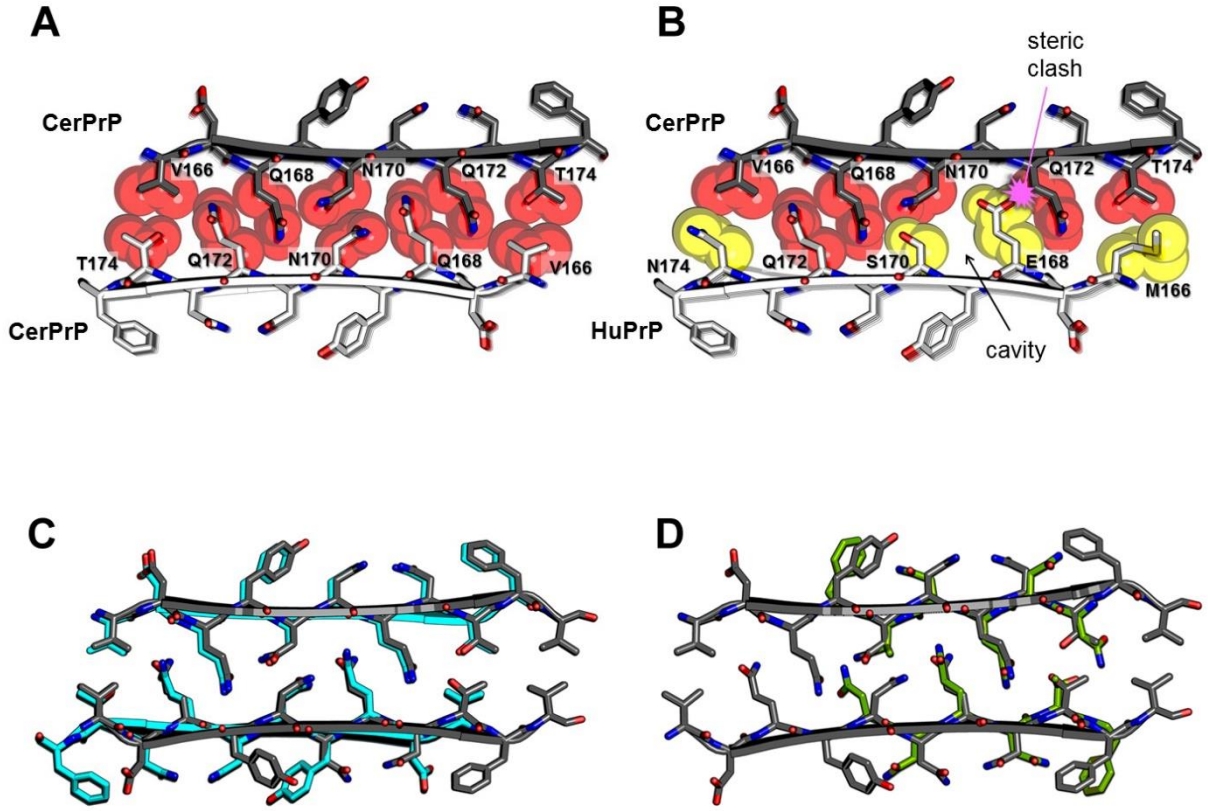

Supplemental Figure 6. An analysis of class 1 and class 3 zipper models. Due to the semi-palindromic sequence of the cervid β2-α2 loop, a class 1 zipper model shows side chain interactions similar to the class 3 model (Figure 6) and is also in good agreement with experimental results (Figure 5). (**A**) A class 1 zipper model also shows steric clashes and gaps at the zipper interface. Atomic space-filling model of the class 1 zipper illustrates the view down the fibril axis. The left panel shows the two β-sheets (gray or white backbone) composed of repeating cervid β2-α2 loop segments. (**B**) The apposition of the donor cervid β2-α2 loop segment (gray) with the recipient human loop segment (white) containing human-specific residues M166, E168, S170, and N174 (yellow). The side chain interactions reveal steric clashes between human E168 and cervid Q172, and a cavity located near the 170 position expected to hinder conversion. (**C**) Class 1 (cyan) and class 3 (gray) zipper models of elk PrP are overlayed, illustrating the similarities in the side chain interface between donor and recipient beta-sheets. (**D**) Elk PrP side chain interactions in the class 3 zipper model align closely with the crystal structure of the elk prion segment NNQNTF. When overlayed, the side chain interactions between the pair of beta-sheets in the model (VDQYNNQNTFV, gray) are similar to that reported in the cervid PrP170-175 crystal structure (NNQNTF, PDB code 3FVA, green)**.**

Supplemental Videos, 1-2. (**1**) A CWD-inoculated Tg(HuPrP$^{elk166-174}$) mouse at 315 dpi shows clinical signs of neurologic disease including kyphosis, lack of movement, and wide-leg stance. (**2**) A CWD-inoculated Tg(HuPrP) mouse at 316 dpi shows normal behavior.

Supplemental Table 1. Computational analysis of the class 3 zipper model correlates with experimental results of CWD-driven conversion[1].

Model or Crystal structure	Sequence of the donor PrP loop[2]	Sequence of the recipient PrP loop[2]	Rosetta Energy[3] (kcal/mol)	Shape Comple-mentarity[4]	Buried Surface Area[5] (Å)	CWD Conversion Efficiency
Elk : Elk	VDQYNNQNTFV	VDQYNNQNTFV	-29	0.72	144	100%
Elk : Hu	VDQYNNQNTFV	MDEYSNQNNFV	-*	-*	-*	1-2%
Elk : Hu-166V	VDQYNNQNTFV	VDEYSNQNNFV	-*		-*	1-2%
Elk : Hu-168Q	VDQYNNQNTFV	MDQYSNQNNFV	-29		147	26%
Elk : Hu-170N	VDQYNNQNTFV	MDEYNNQNNFV	-*	-*	-*	17%
Elk : Hu-174T	VDQYNNQNTFV	MDEYSNQNTFV	-*	-*	-*	1-2%
Elk : Hu-168Q,170N	VDQYNNQNTFV	MDQYNNQNNFV	-30	0.67	148	97%
Elk : Hu-166V,168Q,170N	VDQYNNQNTFV	VDQYNNQNNFV	-30	0.68	148	89%
Elk : Hu-168Q,170N,174T	VDQYNNQNTFV	MDQYNNQNTFV	-28	0.65	147	9%
Elk : Elk Crystal structure	NNQNTF	NNQNTF	-18	0.77	99	N/A

1. The efficiency of conversion can be correlated with the packing of donor and recipient loops in our model of the steric zipper interface. The N174 (human) - T174 (elk) side chains make more favorable interactions than the T174 (elk) – T174 (elk) side chains, which can explain the inhibitory effect of the N174T substitution in the CWD conversion of HuPrP.
2. The donor and recipient beta sheets contain five beta-strands in our calculation.

3. Full-atom Rosetta interaction energy per beta-strand. Total energy is the sum of physical meaningful terms, including non-bond energy, salvation, H-bond energy and other statistical potentials. Note, Dunbrack side chain energy is omitted, because this statistical potential derived from globular proteins is not suitable in amyloid fibril calculation. A lower energy indicates a more favorable interaction at the zipper interface.
4. Shape complementarity score of the zipper interface between two beta-sheets is calculated by CCP4 package. Each beta sheet contains five beta-strands.
5. Buried solvent-accessible surface (SAS) area per beta-strand.
*Due to the steric clash between E168(Hu) and Q168(elk) side chains (as shown in Figure 6), our calculation requires several optimization rounds to reach a reasonable energy score for the model. However, the optimized model has a partially open structure at the positions 166-168, different from tightly packed interfaces of other models and crystal structures.